Enhancing flexibility and strength-to-weight ratio of polymeric stents
A new variable-thickness design approach

Khatami, Mohamad; Doniavi, Ali; Abazari, Amir Musa; Fotouhi, Mohammad

DOI
10.1016/j.jmbbm.2023.106262

Publication date
2023

Document Version
Final published version

Published in
Journal of the mechanical behavior of biomedical materials

journal of the mechanical behavior of biomedical materials 150 (2024) 106262

Contents lists available at ScienceDirect

Journal of the Mechanical Behavior of Biomedical Materials

journal homepage: www.elsevier.com/locate/jmbbm

Enhancing flexibility and strength-to-weight ratio of polymeric stents: A new variable-thickness design approach

Mohamad Khatami [a], Ali Doniavi [a], Amir Musa Abazari [a,*], Mohammad Fotouhi [b]

[a] Department of Mechanical Engineering, Faculty of Engineering, Urmia University, Urmia, Iran
[b] Department of Materials, Mechanics, Management & Design (3MD), Faculty of Civil Engineering and Geosciences, Delft University of Technology, Delft, the Netherlands

ARTICLE INFO

Keywords:
Stent
Variable-thickness
Flexibility
3D printing
Finite element method

ABSTRACT

This paper presents a new design strategy to improve the flexibility and strength-to-weight ratio of polymeric stents. The proposed design introduces a variable-thickness (VT) stent that outperforms conventional polymeric stents with constant thickness (CT). While polymeric stents offer benefits like flexibility and bioabsorption, their mechanical strength is lower compared to metal stents. To address this limitation, thicker polymer stents are used, compromising flexibility and clinical performance. Leveraging advancements in 3D printing, a new design approach is introduced in this study and is manufactured by the Liquid Crystal Display (LCD) 3D printing method and PLA resin. The mechanical performance of CT and VT stents is compared using the Finite Element Method (FEM), validated by experimental tests. Results demonstrate that the VT stent offers significant improvements compared to a CT stent in bending stiffness (over 20%), reduced plastic strain distribution of expansion (over 26%), and increased radial strength (over 10%). This research showcases the potential of the VT stent design to enhance clinical outcomes and patient care.

1. Introduction

Cardiovascular diseases cause 40% of annual deaths in the European Union, and their approximate cost is 196 billion euros (Rebelo et al., 2015). Coronary arteriosclerosis is one of the most common cardiovascular diseases (Hansson, 2005; Shen et al., 2021b,d; Wang and Butany, 2017). This type of disease can be treated with drugs such as anticoagulants, antiplatelet agents, or with surgical procedures. Cardiovascular stents are used in a surgery called angioplasty (Okereke et al., 2021) and have tubular and perforated structures (Chen et al., 2015). They are implanted in the blood vessels to keep the vessels open and restore the normal flow of blood. To be used as implantable medical equipment, stents must have several essential characteristics, such as mechanical resistance, radiopacity, longitudinal flexibility, high radial expansion, corrosion resistance, biocompatibility, and easy control (Saraf and Yadav, 2018).

Stents can be made of different materials, but metal stents, especially stainless steel, is the most common commercial stents due to their excellent mechanical properties. However, metal stents have some limitations such as low radiopacity, corrosion, restenosis, and bleeding complications (Saraf and Yadav, 2018). Restenosis occurs in approximately 30% of patients after surgery and is associated with a high mortality rate and healthcare costs (Park et al., 2019). One of the main problems caused by restenosis is damage to the vessels by metal stent rods and, as result, the immune and inflammatory response of the human body. In order to minimize the problems associated with metal stents, new materials such as polymers are being developed (Hu et al., 2015; Roopmani et al., 2019; Yang et al., 2013). On the other hand, developing polymer-based vascular scaffolds requires a new structural geometry, because these polymer materials have significantly less radial strength than metal alloys (Guerra et al., 2018). For this reason, polymer stents are thicker than the metal ones, which reduces their flexibility.

Stent flexibility is one of the most influential parameters for stent implantation in coronary arteries; a stent with high flexibility quickly passes through tortuous arteries and reaches the occlusion site (Wu et al., 2007). The stent must conform to the shape of the vessel after being implanted in the vessel (Foin et al., 2013). An ideal stent should provide the radial resistance needed to restore blood flow and flexibility. In order to investigate the flexibility of the stent, the finite element method (FEM) can be used, which is a valuable method for the analysis of the stent structure and provides much information in studying and optimizing the design of the stents (Bobel et al., 2015; Li et al., 2009;

* Corresponding author.
E-mail addresses: m.khatami@urmia.ac.ir (M. Khatami), a.doniavi@urmia.ac.ir (A. Doniavi), am.abazari@urmia.ac.ir (A.M. Abazari), M.Fotouhi-1@tudelft.nl (M. Fotouhi).

https://doi.org/10.1016/j.jmbbm.2023.106262
Received 11 September 2023; Received in revised form 17 November 2023; Accepted 20 November 2023
Available online 24 November 2023
1751-6161/

Shen et al., 2019). Azaouzi et al. (2013) investigated the effect of stent design, especially bridges, on the flexibility of the stent by using the finite element and showed that the connecting elements have the most significant effect on the structural behavior of the stent. Mori et al. (Mori and Saito, 2005) developed an optimal method to determine the bending stiffness of the stent. They used the four-point bending test to check the flexibility of the stent and the FEM to evaluate the effect of the stent structure on the flexibility of the stent with different link structures. Grogan et al. (2012) investigated the mechanical properties of degradable metal stents using bench-testing simulation and showed that by changing the design parameters such as width and thickness, these stents can be replaced with permanent stents.

As a flexible manufacturing method, 3D printing has made it possible to create creative designs in the field of stents (Tofail et al., 2018). Wang et al. (2021) investigated the 3D printing of polymer stents and their longitudinal deformation. They concluded that by optimizing the design, the longitudinal deformation of the stent can be prevented when it is placed in the vessel. LCD 3D printers use a liquid crystal display screen to selectively cure a layer of photopolymer resin. Other methods such as molding has been applied for manufacturing polymeric stents but some limitations have been recorded. Difficulty making micro-devices with complex geometries and the importance of flowability at different temperatures are crucial factors that may affect the uniformity of stents (Ang et al., 2017; Park et al., 2007; Xu et al., 2021). LCD method can create detailed and intricate models with smooth surfaces and fine details.

In the case of polymer stents, bridges are crucial for enhancing the flexibility of stents, while the struts contribute to the stent's radial strength (Qiu et al., 2018). Padilla et al. (2001) design a stainless steel stent with varying link and bar thickness to enhance the flexibility, strength and radiopacity. They used laser to produce this stent. In this study, a novel polymer stent design was proposed using this technique, called variable-thickness (VT) stent, which has a variable thickness in the bridge and strut. LCD 3D printer was used to fabricate the stents. Bending stiffness and equivalent plastic strain distribution of the VT stent were investigated with experimentally validated FEM and compare with CT stent.

2. Materials and methods

2.1. Material properties

Poly lactic acid (PLA) resin (supplied by Shenzhen Esun Industrial Co., Ltd) was used as the stent material. In polymers, the mechanical response is directly related to the manufacturing process. As a result, it is necessary to extract accurate mechanical properties of the stent material, such as Young's modulus and yield strength. These properties are used to simulate the stent with FEM. For this purpose, three PLA specimens were first fabricated using an LCD 3D printer, according to ASTM D638 type IV standard (Fig. 1). Subsequently, a uniaxial tensile test was conducted on the 3D printed specimens using a universal testing machine (SANTAM STM-150).

During the uniaxial tensile test, both ends of the sample were attached to the grip, and testing was performed at a velocity of 5 mm/min until the final failure (Fig. 1). Standardized Mean Difference (SMD) between the results of the tests is −0.047, indicating no significant difference between them. Fig. 2 shows mean values of the stress-strain curves of the samples. According to this experimental curve, the yield stress and Young's modulus of the PLA specimen are 30 Mpa and 1.36 GPa, respectively.

2.2. Stent design

A strut-bridge stent (Wang et al., 2017) was investigated in this study, called a constant-thickness (CT) stent. Fig. 3 shows the planar view and geometrical parameters of this stent. These parameters play an essential role in the mechanical properties of the stent.

Table 1 shows the specifications of this stent.

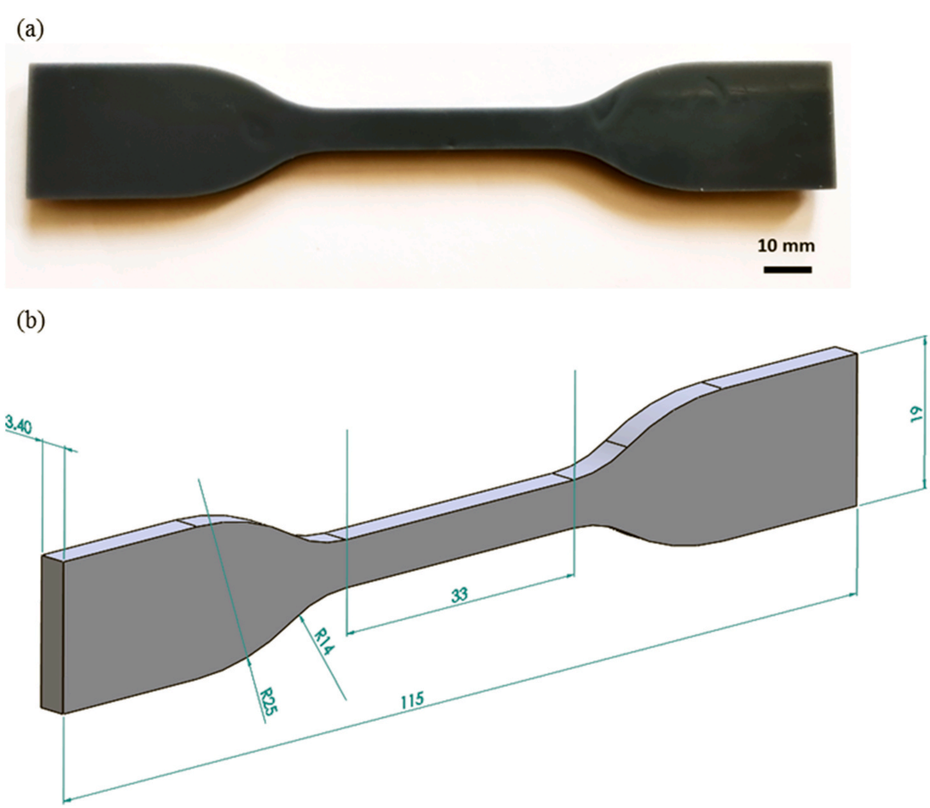

Fig. 1. ASTM D638 type IV specimen: (a) 3D printed with LCD method, (b) schematic view.

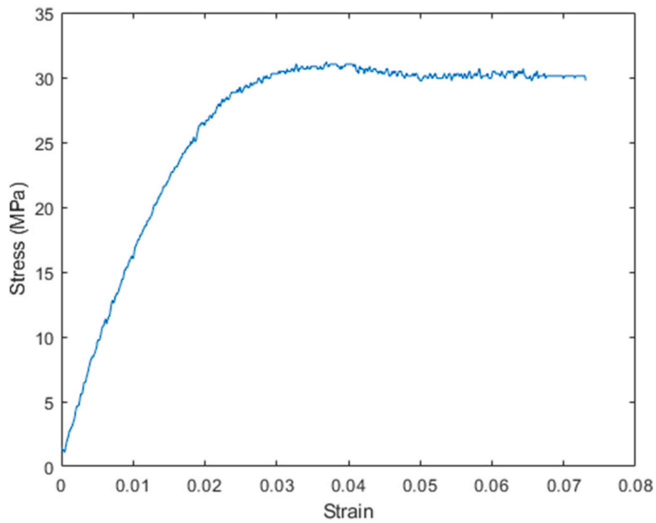

Fig. 2. Stress-strain curve of the PLA specimen.

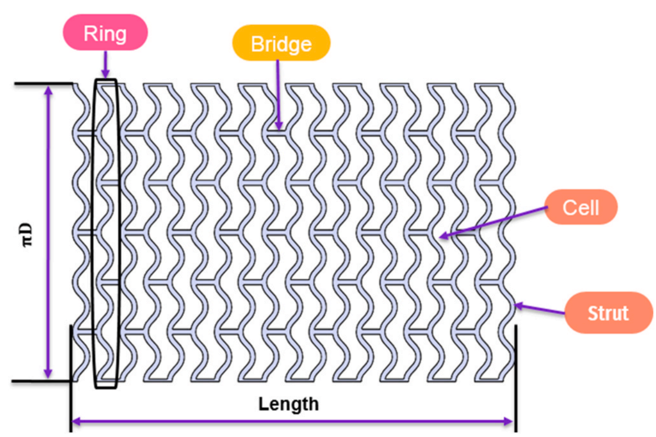

Fig. 3. Planar view and Geometrical parameters of the stent.

Table 1
The polymer stent geometry (Wang et al., 2017).

Stent	Length (mm)	Outer Diameter (mm)	Bridge Width (mm)	Strut Width (mm)	Stent Thickness (mm)
Polymer	18	3.40	0.18	0.2	0.15

The VT stent is a new design that is proposed in this paper, which can be produced with the advancement in technology and the emergence of 3D manufacturing process (Khatami et al., 2023). In a CT stent, the thickness of the bridges remain constant throughout the length of the stent, while in a VT stent, the thickness of the bridges can vary. In this research, polymer stents with CT and VT designs were modeled using Table 1 and SolidWorks software. Previous researches has shown that when the thickness of a stent exceeds 0.1 mm, the risk of late restenosis significantly increases (Holzapfel et al., 2005; Iantorno et al., 2018; Kolandaivelu et al., 2011; Lipinski et al., 2016). As a result, the VT stent has a bridge thickness of 0.1 mm. Fig. 4 shows the schematic view of these stents with two rings and a detail view of the VT stent.

2.3. Stent fabrication

To manufacture the VT coronary stent, a high-precision 3D printing method was needed to create a variable thickness along the length of the stent. For this purpose, LCD 3D printing machine (ALTON3D) was used to fabricate the CT and VT stents. Fig. 5 shows the printed view of the CT and VT stents that is observed using an optical microscope (Dewinter Optical Inc., DMI Victory).

2.4. Finite element modeling

Computer simulation is a valuable support tool for evaluating the effective parameters for in the design of the stents (Salavatidezfouli et al., 2023; Shen et al., 2021c). It significantly saves time and money compared to similar laboratory methods and provides more detailed information. The mechanical behavior of polymer stents can be evaluated using FEM. The Abaqus software is used for the simulation. Fig. 6 shows the FEM of the three-point bending, expansion and crimping process of the stent. The choice of a constitutive modeling approach for bioresorbable polymers like PLA can range from intricate methods that necessitate numerous material constants to straightforward approaches based on general elastic-plastic properties (Donik et al., 2022). According to Fig. 2, a general elastic–plastic material model was used for PLA stents.

The flexibility was investigated for the CT and VT stents under three-point bending test according to ASTM F2606-08 standard. In this standard, for a stent length of 18 mm, it is recommended to use a span length of 11 mm, and the allowable deflection within this span must not exceed 2.2 mm. This gives a reasonable range for simulation considering the real life deflection ranges the stent is supposed to be used. Simulation setup of this test is shown in Fig. 7. This test consists of two lower static support and one upper load applicator which were modeled as the parallel rigid cylinders with a diameter of 6.35 mm. The distance between the two lower static supports, known as the span length, is equal to 11 mm. The load applicator was used to apply the force up until 1.5 mm deflection of the stent, and the bending flexibility was obtained by evaluating the slope of force-versus-deflection plot.

To simulate the stent expansion process, two circumferential rings of the stent was considered and the following steps were established: expanding (step 1), and spring-back after expanding (step 2). In step 1, the diameter of the stent was increased from 3.40 to 3.9 mm. The balloon was then removed, and the stent spring-back after expansion at step 2. A free-cylinder model was used to analyze the stent expansion process, with the balloon considered as a cylindrical shape under displacement control (Gervaso et al., 2008). For this purpose, a balloon with a linear elastic model was utilized. The balloon has a Poisson's ratio of 0.3 and a Young's modulus of 900 MPa.

To evaluate the stent radial strength, the collapse pressure of the short stent geometry (consisting of two circumferential rings) in its deployed state was measured. To achieve this goal, a crimping tool with a Poisson's ratio of 0.4 and a Young's modulus of 1000 MPa (Grogan et al., 2012), reduced the outer diameter of the stent to 1.7 mm, after step 2 in the expansion process. The collapse characteristics of the stent were assessed by analyzing the relationship between pressure and diameter. The stent's outer diameter (D) was determined under different applied pressures. The pressure at which a 10% reduction in diameter occurred, compared to the initial unloaded stent outer diameter (D_0), was considered as an indicator of the stent's radial strength (Shen et al., 2021a).

The balloon was modeled as four-node bilinear quadrilateral (S4R) element. A quadratic tetrahedral element (C3D10) with 10 nodes was used to mesh the stent geometry. In order to find the optimal mesh size, a mesh sensitivity analysis was performed that balances accuracy of results with computational efficiency. As shown in Fig. 8, during the three-point bending test simulation a mesh size of 0.1 mm was identified as stable and further reducing the mesh size would have no significant impact on the result. Consequently, it was selected for simulating the stent. Stent simulation procedure was analyzed in Abaqus/standard using FEM.

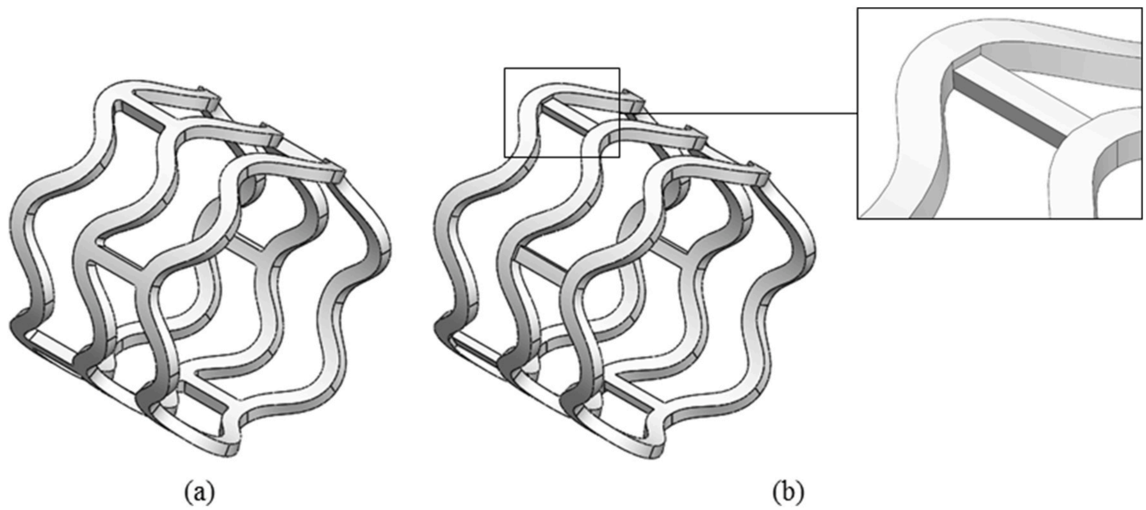

Fig. 4. Schematic view of the polymer stents (a) constant-thickness (CT), (b) variable-thickness (VT) with Detail view.

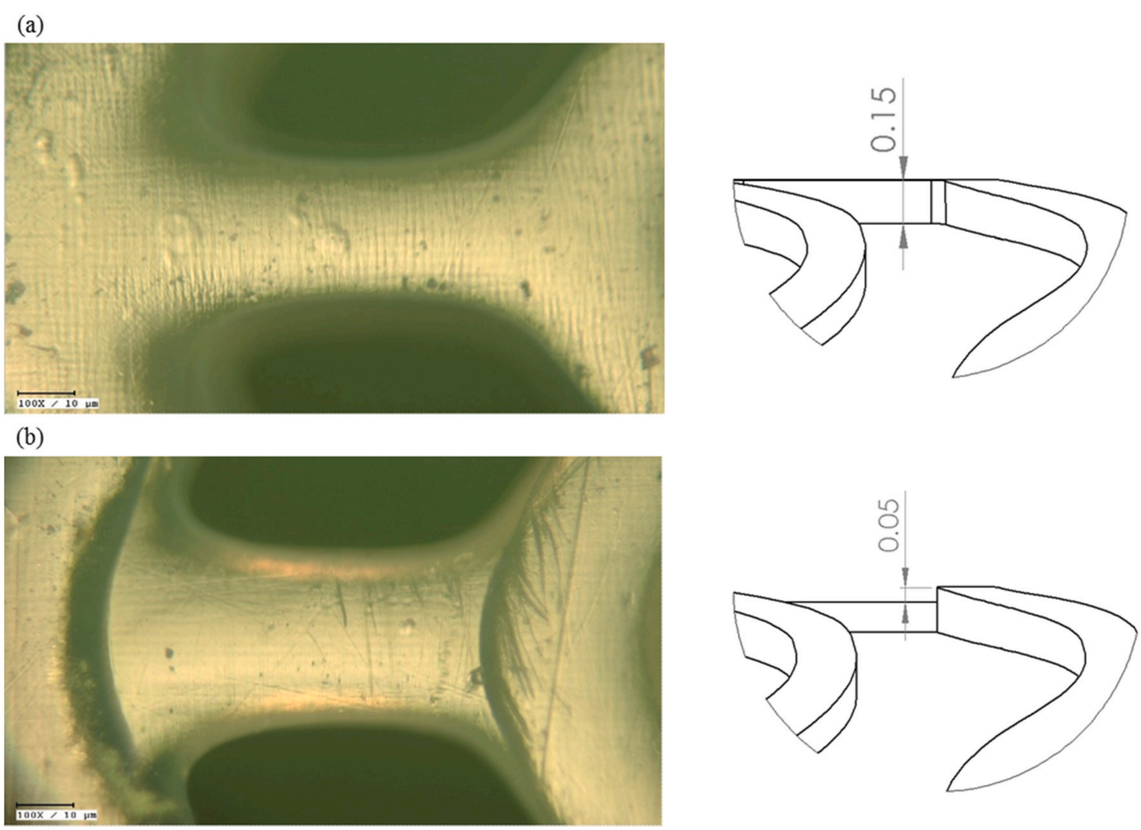

Fig. 5. 3D printed stent: (a) constant-thickness, (b) variable-thickness.

2.5. *Experimental investigating*

Fig. 9 shows the three-point bending flexibility test was performed on testing machine (FP4ME). The experimental results are conducted in the same conditions as the FEM, and are used to validate the FEM.

3. Results

3.1. *Verification*

Fig. 10 illustrates the force-deflection curve for both the simulation and experimental three-point bending test of the VT stent. It shows the relationship between the amount of force applied to the stent and the amount it bends, allowing for comparison between the simulated results and the experimental results. During the three-point bending process, the curve was non-linear and caused an elastic-plastic deformation. When the deflection was less than 0.4 mm the flexibility of the stent can be determined by calculating the slope of the linear (elastic) portion of the force-deflection curve. As shown in Fig. 10, when analyzing the slope of simulation and experimental force-deflection curve within their elastic region, the variation in their results does not exceed 5%.

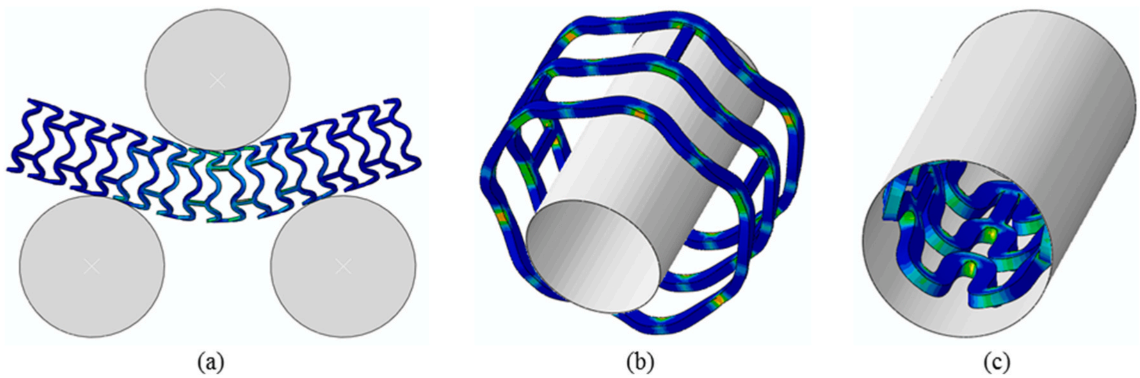

Fig. 6. Finite element model of the stent (a) three-point bending, (b) expansion process, (c) crimping process.

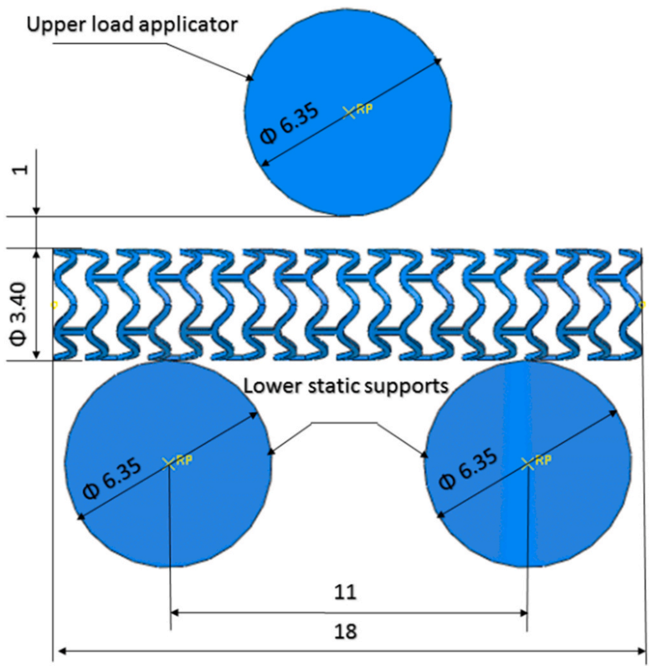

Fig. 7. Three-point bending test of the stent.

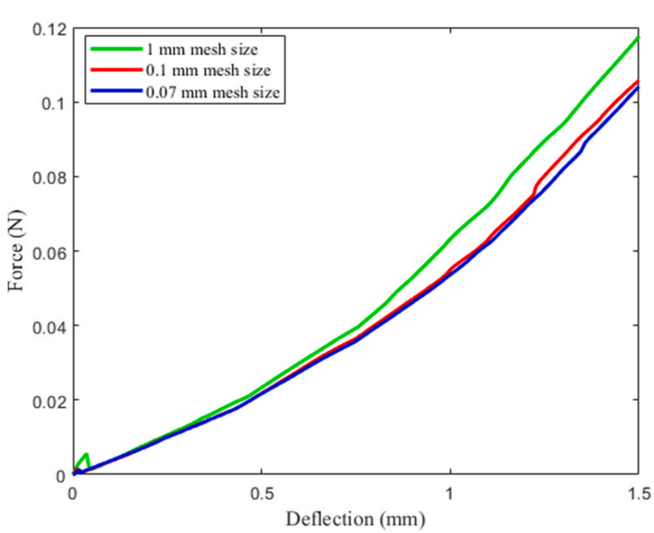

Fig. 8. Mesh sensitivity analysis: Force-deflection curve for different mesh sizes during the three-point bending test simulation of the stent.

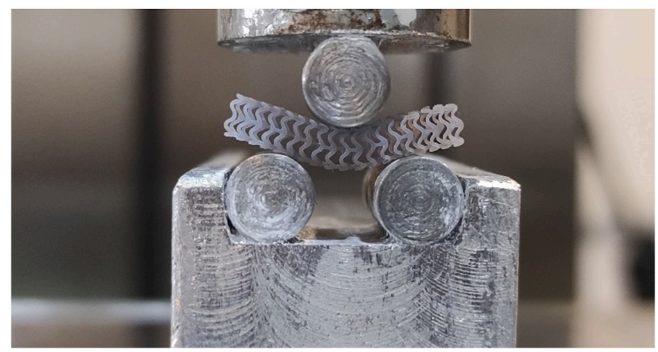

Fig. 9. Experimental test of the three-point bending process.

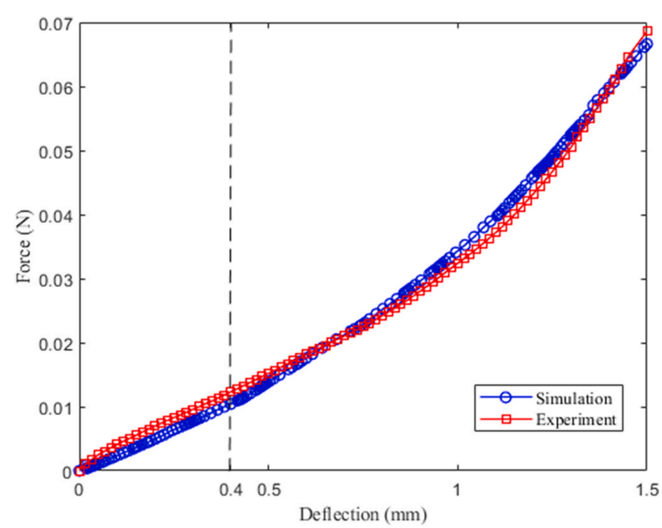

Fig. 10. Force-deflection curve for both the simulation and experimental three-point bending test for the VT stent.

3.2. Radial strength

The reduction in the outer diameter (D) of the stent compared to its unloaded diameter (D_0) caused by an external applied pressure are displayed in Fig. 11. The pressure needed to cause a 10% decrease in diameter was considered as the stents' radial strength. The prediction indicated that the CT and VT stents had collapse pressures of 90 kPa and 99 kPa, respectively, which significantly surpasses the recommended minimum collapse pressure of 40 kPa for coronary stents (Li et al., 2014).

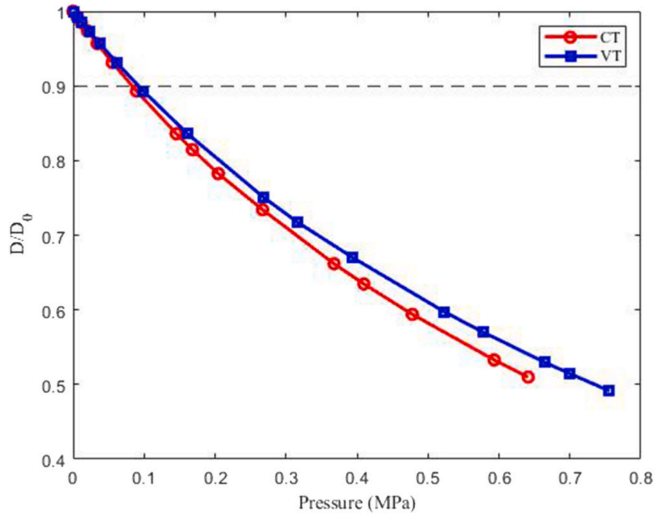

Fig. 11. Radial strength of the CT and VT stents during external applied pressure.

Equivalent plastic strain (PEEQ) distribution is a measure of the total plastic strain that occurs throughout the deformation process.

As depicted in Fig. 12, when crimped to an outer diameter of 1.7 mm, the maximum equivalent plastic strain of crimping ($PEEQ_{crimp}$) in the VT configuration was 0.933, which was lower than the initial configuration's equivalent plastic strain of 1.118.

3.3. Bending stiffness

A stent is considered more flexible when the slope of the curve is lower, indicating that it can bend or deform more easily when subjected to a certain level of force. The evaluation of a cantilever beam's resistance to bending deformation involves considering its bending stiffness in relation to free bending length, deflection, and bending force (Schmidt et al., 2009). In this study, we propose a similar method for measuring the bending stiffness of a stent modeled as a simply supported beam, with a concentrated force applied to its midpoint. The bending stiffness EI (Eq. (1)) is a function of fixed span length l, deflection f, and concentrated bending force F.

$$\text{Bending Stiffness } EI = \frac{F \cdot l^3}{48f} \tag{1}$$

Fig. 13 shows the force-deflection curve of the CT stent and VT stents. The bending stiffness at a deflection of 1.5 mm for CT stent was determined to be 1.84 N mm^2. This is greater than the bending stiffness of 1.47 N mm^2 in VT stent. Stents with higher bending stiffness at a given deflection are less flexible when bent. As a result, the VT stent is more flexible than the CT stent.

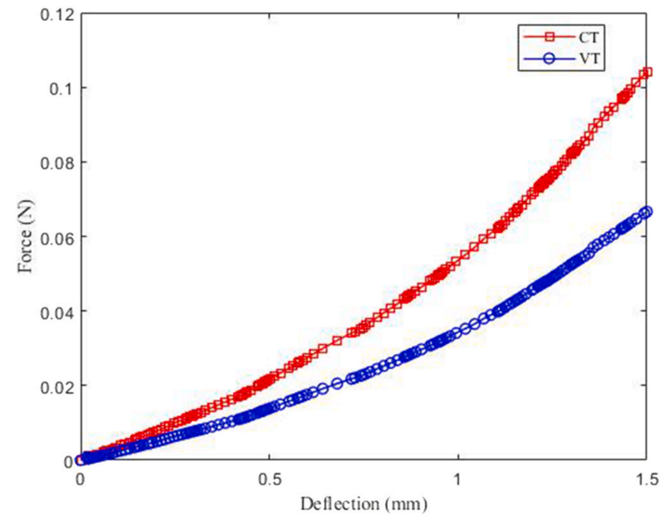

Fig. 13. Force-deflection curve of the CT and VT stent.

3.4. Stent expansion and spring-back

Fig. 14 shows the structural change and the equivalent plastic strain distribution of expansion ($PEEQ_{expand}$) for both the expanded Initial CT stent and the expanded VT stent.

In Fig. 14, it was shown that the maximum equivalent plastic strain in the VT stent was 0.517 when the stent spring-back after being expanded to the outer diameter of 3.9 mm. This is less than the maximum equivalent plastic strain of 0.704 in the initial configuration (CT stent).

The amount of expansion of a stent applied to a specific blood vessel is determined by the radial recoil ratio. If the radial recoil ratio is too high, the stent will over-expand, causing significant strain on the arteries, which can lead to a high risk of mechanical injury and subsequent inflammation. The definition of the radial recoil ratio after expanding involves measuring the decrease in inner diameter between two stages. During the first stage, the stent was expanded to reach a specific inner diameter. In the second stage, the stent underwent a spring-back effect after being expanded (Eq. (2)).

$$\text{Radial Recoil Ratio after Expanding} = \frac{ID_{\exp\ and} - ID_{\exp\ and\ recoil}}{ID_{\exp\ and}} \tag{2}$$

Table 2 shows the radial recoil ratio of the CT and VT stents, after the stent had been expanded to an inner diameter of 3.77 mm. Both stents

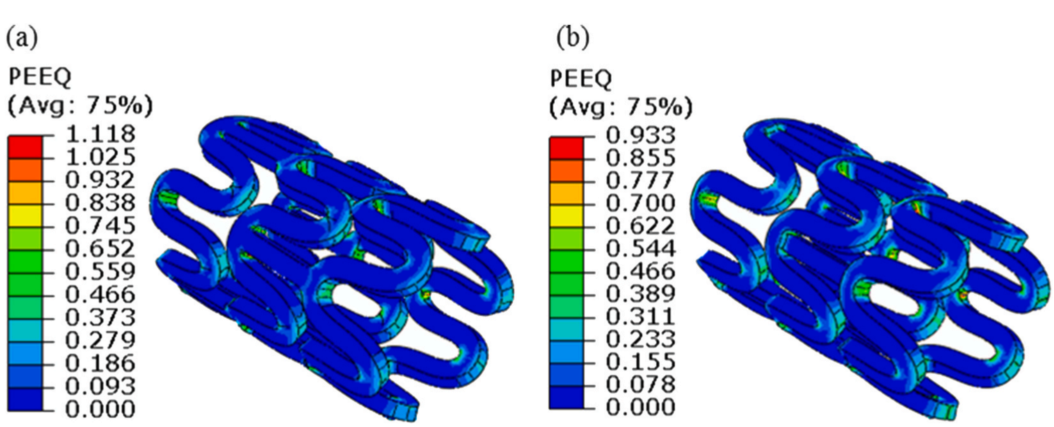

Fig. 12. Equivalent plastic strain of (a) CT (b) VT stents after crimped to outer diameter of 1.7 mm.

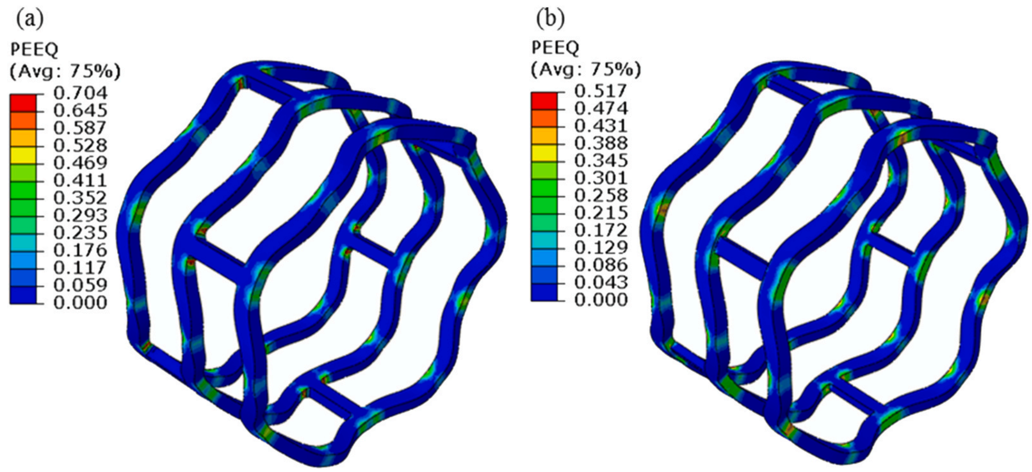

Fig. 14. Equivalent plastic strain of (a) initial (CT) and (b) VT stents after spring-back with the expanded outer diameter of 3.9 mm.

Table 2
Radial recoil ratio of the CT and VT stents.

Stent Design	CT	VT
Expanded to ID (mm)	3.7	3.7
Recoiled to ID (mm)	3.6	3.6
Radial recoil ratio (%)	2.7	2.7

have an identical radial recoil ratio, which is approximately equivalent to 2% in value.

4. Discussion

Mechanical properties are critical for stents, as they need to withstand the dynamic forces exerted on them within the arterial environment. The stent must possess sufficient radial strength to maintain vessel patency and prevent recoil, while also exhibiting flexibility to accommodate vessel movement during cardiac cycles. The selection of an appropriate polymer and stent design plays a crucial role in achieving these mechanical requirements. In this study, we aimed to develop an optimized polymer stent for improved performance in terms of mechanical properties. Our findings suggest that the incorporation of specific polymers and fabrication techniques can significantly enhance the overall performance of stents, making them more suitable for clinical applications.

4.1. Radial strength

In order to enhance the radial strength, currently existing biodegradable polymer stents such as ABSORB BVS have high thicknesses of 157 μm (Li et al., 2022a). Studies have shown that an increased strut thickness is associated with a higher risk of late thrombotic stenosis (Prithipaul et al., 2018). Consequently, the latest generation of stents, whether polymer-based or metallic, is moving towards thinner struts. However, thin-walled stents may face challenges such as insufficient radial strength or stress concentration. To address these concerns, structural optimization design can be employed. In this regard, we propose a VT stent with a thickness of 100 μm in bridge. This structure aims to simultaneously meet the design requirements of stents, including high radial strength and flexibility. In contrast to the CT stent, the VT stent has demonstrated a notable improvement in radial strength, exhibiting a substantial increase of 10.0% (measured at 99 kPa compared to 90 kPa). The reason for this is the interaction between the crimping tool and the stent's contact area. The pressure exerted on the external surface of the stent by the crimping tool is calculated using Eq. (3) (Bobel et al., 2015).

$$p = \frac{F_r}{A_c} \tag{3}$$

In this relation, F_r is the radial reaction force and A_c is the area of the contact surface of the stent (surface coverage area), which is calculated from Eq. (4).

$$A_c = A_{strut} + A_{bridge} \tag{4}$$

In this equation, A_{strut} represents the surface area of the struts, and A_{bridge} is the surface area of the bridges that comes into contact with the inner surface of the crimping tool. In the case of VT stent, when pressure is applied from the crimping tool to the outer surface of the stent, only the strut rings, which play a primary role in the stent's radial strength, are engaged (Fig. 15(b)). However, in the CT stent, both the bridges and struts are involved simultaneously (Fig. 15(a)). As a result, the surface coverage area of the VT stent is smaller than that of the CT stent. Consequently, according to Eq. (4), the VT stent experiences higher applied and collapse pressures.

In order to evaluate the performance of the CT and VT stents, their characteristics were compared to those of other commercially available stents (Table 3).

The Absorb BRS, fabricated from PLLA, the magnesium-based Magmaris BRS, the Absorbable magnesium Scaffold (AMS) Magic, and the CT stents all exhibit a greater thickness. In contrast, the thickness of the VT stent is similar to that of the permanent metallic DES MultiLink8 (ML8)/Xience Xpedition (Abbott Vascular) stent, which helps reduce the rate of late thrombotic stenosis. As shown in Table 3, all the stents have the radial strength above the critical threshold for the coronary stents (40 kPa).

Additionally, when compared to the CT stent, the VT stent shows high performance in terms of $PEEQ_{crimp}$ (1.118 compared to 0.933). As a result, the VT stent, undergoes more uniform deformation during the crimping. This can lead to a reduction in dog boning rate and a decrease in high-stress regions (Li et al., 2022b). Fig. 15 shows the stress distribution in the VT and CT stents in the high stress concentration regions. Low-stress areas can be found around the junction between the bridge and strut in the CT stent (Fig. 16(a)). Over the long term, these areas increase the local stent degradation rate, leading to a reduction in the stent performance (Chen et al., 2019). In regions where the stress concentration is particularly high, the adjustment in the bridge thickness of the VT stent has helped to distribute the stress more evenly (Fig. 16(b)), so it is expected that the VT design would outperform the CT in the fatigue life due to the reduced stress concentration. However further research needs to be performed in this direction to evaluate the long term degradation process.

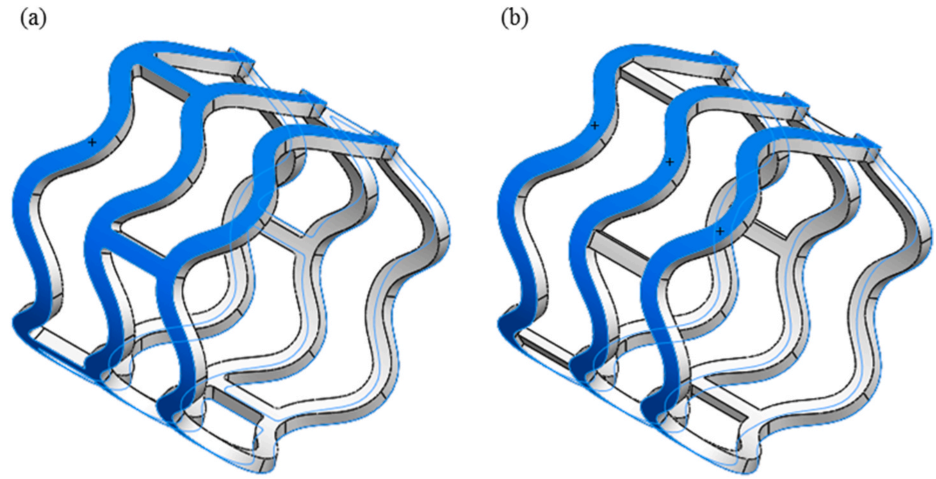

Fig. 15. Contact surface area of (a) CT and (b) VT stents.

Table 3
Comparing the characteristics of the CT and VT stents in relation to Absorb, Magmaris, and ML8/Xience Xpedition stents.

Stent configuration	Thickness (mm)	Width (mm)	Radial Strength (kPa)
Absorb BVS (Barkholt et al., 2020)	0.157	0.191	140
Magmaris (Barkholt et al., 2020)	0.150	0.150	180
AMS MAGIC (Erbel et al., 2007)	0.165	0.080	80
ML8/Xience Xpedition (Jinnouchi et al., 2019)	0.089	0.089–0.112	160
CT	0.15	0.180	90
VT	0.1–0.15	0.180	99

4.2. Bending stiffness

Stent stiffness can influence the amount of force required for deployment. Stiffer stents typically require higher deployment forces because they offer more resistance to expansion. As a result, highly stiff stents may transmit excessive mechanical stress to the surrounding tissue. It can cause injury to the vessel wall. This injury can activate the body's natural healing response. One of the key factors contributing to restenosis is the proliferation of smooth muscle cells. In response to the injury and inflammation, these cells migrate to the site of injury and begin to reproduce. The overgrowth of the smooth muscle cells, known as neointimal hyperplasia, can lead to the re-narrowing of the vessel lumen, causing restenosis (Schwartz et al., 1998; Serruys et al., 1994). The flexibility of the stent depends on its bridges and has an inverse relationship with the stent's stiffness (Chen et al., 2020; Khatami et al., 2024). The VT stent, with its thinner stent bridge (100 μm compared to 150 μm) and smaller bending stiffness (1.47 N mm^2 compared to 1.84 N mm^2), is anticipated to enhance flexibility and reduce restenosis. The flexibility improves the stent's ability to conform to the natural curvature and movement of blood vessels within the body. This is important because blood vessels are not rigid structures and can undergo dynamic changes due to factors such as body movement, pulsatile blood flow, and vessel diameter variations.

4.3. Stent expansion and spring-back

The $PEEQ_{expand}$ of the VT stent was found to be smaller when compared to the initial CT stent (0.517 vs. 0.704). This is because of a significant change in the location of the maximum equivalent plastic strain (Fig. 17). In the initial stent, the maximum equivalent plastic strain was at inside surface of a bow, while in the VT configuration, it was at a different location in the connection point of the Strut and bridge.

The radial recoil ratio of the VT stent is similar to that of the CT stent (2%). Therefore, it was recommended to have an over-expansion of at least 0.1 mm, regardless of the force exerted by the interaction between

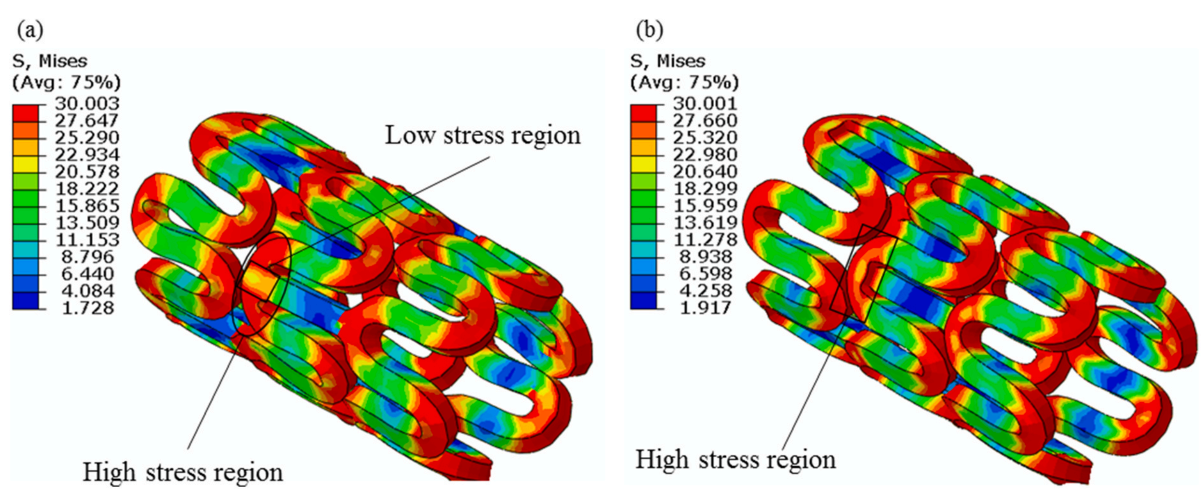

Fig. 16. Low and high stress regions in stress distribution of (a) CT (b) VT stents after crimped to the outer diameter of 1.4 mm.

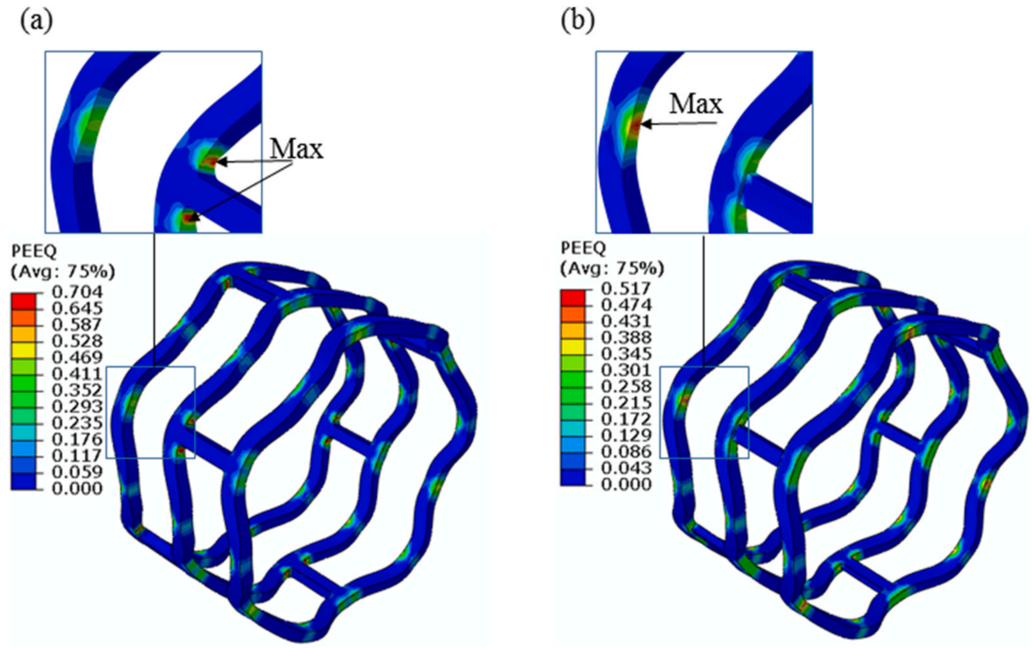

Fig. 17. Location of maximum equivalent plastic strain (a) initial (CT) and (b) VT stents after spring-back with the expanded outer diameter of 3.9 mm.

the stent and the artery.

5. Conclusions

This study evaluated the performance of a novel VT stent compared with a conventional polymeric VT stent. Experimental three-point bending tests and an experimentally validated FEM were used to characterize the mechanical performance and strain distribution under a three-point bending loading. The following conclusions are drawn:

In comparison to the CT stent, the VT stent demonstrated an enhancement of 10% in radial strength. This improvement in radial strength displays the superior performance and robustness of the VT stent.

The maximum equivalent plastic strain of expansion in the VT stent was reduced by 26.5% in comparison with the CT stent, which is an effective way to minimize damage to the blood vessel.

The bending stiffness of the VT stent was about 20% lower than the CT stent, showing a more flexible behavior of the VT design which is an important factor in improving the performance of the CT stent.

CRediT authorship contribution statement

Mohamad Khatami: Writing – original draft, Visualization, Validation, Software, Investigation, Data curation. **Ali Doniavi:** Supervision, Project administration, Funding acquisition. **Amir Musa Abazari:** Writing – review & editing, Methodology, Investigation, Formal analysis, Conceptualization. **Mohammad Fotouhi:** Writing – review & editing, Conceptualization.

Declaration of competing interest

The authors declare that they have no known competing financial interests or personal relationships that could have appeared to influence the work reported in this paper.

Data availability

Data will be made available on request.

Acknowledgment

This research did not receive any specific grant from funding agencies in the public, commercial, or not-for-profit sectors.

References

Ang, H.Y., Bulluck, H., Wong, P., Venkatraman, S.S., Huang, Y., Foin, N., 2017. Bioresorbable stents: current and upcoming bioresorbable technologies. Int. J. Cardiol. 228, 931–939.
Azaouzi, M., Makradi, A., Belouettar, S., 2013. Numerical investigations of the structural behavior of a balloon expandable stent design using finite element method. Comput. Mater. Sci. 72, 54–61.
Barkholt, T., Webber, B., Holm, N.R., Ormiston, J.A., 2020. Mechanical properties of the drug-eluting bioresorbable magnesium scaffold compared with polymeric scaffolds and a permanent metallic drug-eluting stent. Cathet. Cardiovasc. Interv. 96, E674–e682.
Bobel, A.C., Petisco, S., Sarasua, J.R., Wang, W., McHugh, P.E., 2015. Computational bench testing to evaluate the short-term mechanical performance of a polymeric stent. Cardiovasc. Eng. Technol. 6, 519–532.
Chen, C., Chen, J., Wu, W., Shi, Y., Jin, L., Petrini, L., Shen, L., Yuan, G., Ding, W., Ge, J., Edelman, E.R., Migliavacca, F., 2019. In vivo and in vitro evaluation of a biodegradable magnesium vascular stent designed by shape optimization strategy. Biomaterials 221, 119414.
Chen, C., Xiong, Y., Li, Z., Chen, Y., 2020. Flexibility of biodegradable polymer stents with different strut geometries. Materials 13.
Chen, W., Habraken, T.C.J., Hennink, W.E., Kok, R.J., 2015. Polymer-free drug-eluting stents: an overview of coating strategies and comparison with polymer-coated drug-eluting stents. Bioconjugate Chem. 26, 1277–1288.
Donik, Ž., Nečemer, B., Glodež, S., Kramberger, J., 2022. Finite element analysis of the mechanical performance of a two-layer polymer composite stent structure. Eng. Fail. Anal. 137, 106267.
Erbel, R., Di Mario, C., Bartunek, J., Bonnier, J., de Bruyne, B., Eberli, F.R., Erne, P., Haude, M., Heublein, B., Horrigan, M., Ilsley, C., Böse, D., Koolen, J., Lüscher, T.F., Weissman, N., Waksman, R., 2007. Temporary scaffolding of coronary arteries with bioabsorbable magnesium stents: a prospective, non-randomised multicentre trial. Lancet 369, 1869–1875.
Foin, N., Di Mario, C., Francis, D.P., Davies, J.E., 2013. Stent flexibility versus concertina effect: mechanism of an unpleasant trade-off in stent design and its implications for stent selection in the cath-lab. Int. J. Cardiol. 164 (3), 259–261.
Gervaso, F., Capelli, C., Petrini, L., Lattanzio, S., Di Virgilio, L., Migliavacca, F., 2008. On the effects of different strategies in modelling balloon-expandable stenting by means of finite element method. J. Biomech. 41, 1206–1212.
Grogan, J.A., Leen, S.B., McHugh, P.E., 2012. Comparing coronary stent material performance on a common geometric platform through simulated bench testing. J. Mech. Behav. Biomed. Mater. 12, 129–138.
Guerra, A.J., Cano, P., Rabionet, M., Puig, T., Ciurana, J., 2018. 3D-Printed PCL/PLA composite stents: towards a new solution to cardiovascular problems. Materials 11.
Hansson, G.K., 2005. Inflammation, atherosclerosis, and coronary artery disease. N. Engl. J. Med. 352, 1685–1695.

Holzapfel, G.A., Sommer, G., Gasser, C.T., Regitnig, P., 2005. Determination of layer-specific mechanical properties of human coronary arteries with nonatherosclerotic intimal thickening and related constitutive modeling. Am. J. Physiol. Heart Circ. Physiol. 289, H2048–H2058.

Hu, T., Yang, J., Cui, K., Rao, Q., Yin, T., Tan, L., Zhang, Y., Li, Z., Wang, G., 2015. Controlled slow-release drug-eluting stents for the prevention of coronary restenosis: recent progress and future prospects. ACS Appl. Mater. Interfaces 7, 11695–11712.

Iantorno, M., Lipinski, M.J., Garcia-Garcia, H.M., Forrestal, B.J., Rogers, T., Gajanana, D., Buchanan, K.D., Torguson, R., Weintraub, W.S., Waksman, R., 2018. Meta-analysis of the impact of strut thickness on outcomes in patients with drug-eluting stents in a coronary artery. Am. J. Cardiol. 122, 1652–1660.

Jinnouchi, H., Torii, S., Sakamoto, A., Kolodgie, F.D., Virmani, R., Finn, A.V., 2019. Fully bioresorbable vascular scaffolds: lessons learned and future directions. Nat. Rev. Cardiol. 16, 286–304.

Khatami, M., Doniavi, A., Abazari, A.M., Fotouhi, M., 2024. Flexibility and geometric optimization of a new structure for a polymer stent with the finite element method. Sharif J. Mech. Eng. 40, 28–41.

Khatami, M., Doniavi, A., Allahyari, S., Feizollahi, M., Abazari, A.M., Fotouhi, M., 2023. Application of 3D printing in pharmaceutical sciences, and evaluation of administration routes for drug-loaded composites. Pharmaceut. Sci. 29, 283–297.

Kolandaivelu, K., Swaminathan, R., Gibson, W.J., Kolachalama, V.B., Nguyen-Ehrenreich, K.-L., Giddings, V.L., Coleman, L., Wong, G.K., Edelman, E.R., 2011. Stent thrombogenicity early in high-risk interventional settings is driven by stent design and deployment and protected by polymer-drug coatings. Circulation 123, 1400–1409.

Li, J., Zheng, F., Qiu, X., Wan, P., Tan, L., Yang, K., 2014. Finite element analyses for optimization design of biodegradable magnesium alloy stent. Mater. Sci. Eng. C 42, 705–714.

Li, N., Zhang, H., Ouyang, H., 2009. Shape optimization of coronary artery stent based on a parametric model. Finite Elem. Anal. Des. 45, 468–475.

Li, Y., Wang, J., Sheng, K., Miao, F., Wang, Y., Zhang, Y., Hou, R., Mei, D., Sun, Y., Zheng, Y., Guan, S., 2022a. Optimizing structural design on biodegradable magnesium alloy vascular stent for reducing strut thickness and raising radial strength. Mater. Des. 220, 110843.

Li, Y., Wang, Y., Shen, Z., Miao, F., Wang, J., Sun, Y., Zhu, S., Zheng, Y., Guan, S., 2022b. A biodegradable magnesium alloy vascular stent structure: design, optimisation and evaluation. Acta Biomater. 142, 402–412.

Lipinski, M.J., Escarcega, R.O., Baker, N.C., Benn, H.A., Gaglia, M.A., Torguson, R., Waksman, R., 2016. Scaffold thrombosis after percutaneous coronary intervention with ABSORB bioresorbable vascular scaffold: a systematic review and meta-analysis. JACC Cardiovasc. Interv. 9, 12–24.

Mori, K., Saito, T., 2005. Effects of stent structure on stent flexibility measurements. Ann. Biomed. Eng. 33, 733–742.

Okereke, M.I., Khalaj, R., Tabriz, A.G., Douroumis, D., 2021. Development of 3D printable bioresorbable coronary artery stents: a virtual testing approach. Mech. Mater. 163, 104092.

Padilla, O.M., Mirizzi, M.S., Wynne, R.L., Callol, J.R., Kitcen, T.L., 2001. Variable Thickness Stent. European patent EP 1189554B1.

Park, J., Kim, J.-K., Park, S.A., Lee, D.-W., 2019. Biodegradable polymer material based smart stent: wireless pressure sensor and 3D printed stent. Microelectron. Eng. 206, 1–5.

Park, J.H., Choi, S.O., Kamath, R., Yoon, Y.K., Allen, M.G., Prausnitz, M.R., 2007. Polymer particle-based micromolding to fabricate novel microstructures. Biomed. Microdevices 9, 223–234.

Prithipaul, P.K.M., Kokkolaras, M., Pasini, D., 2018. Assessment of structural and hemodynamic performance of vascular stents modelled as periodic lattices. Med. Eng. Phys. 57, 11–18.

Qiu, T.Y., Song, M., Zhao, L.G., 2018. A computational study of crimping and expansion of bioresorbable polymeric stents. Mech. Time-Dependent Mater. 22, 273–290.

Rebelo, R., Vila, N., Fangueiro, R., Carvalho, S., Rana, S., 2015. Influence of design parameters on the mechanical behavior and porosity of braided fibrous stents. Mater. Des. 86, 237–247.

Roopmani, P., Satheesh, S., Raj, D.C., Krishnan, U.M., 2019. Development of dual drug eluting cardiovascular stent with ultrathin flexible poly(l-lactide-co-caprolactone) coating. ACS Biomater. Sci. Eng. 5, 2899–2915.

Salavatidezfouli, S., Alizadeh, A.a., Barzegar Gerdroodbary, M., Sabernaeemi, A., Abazari, A.M., Sheidani, A., 2023. Investigation of the stent induced deformation on hemodynamic of internal carotid aneurysms by computational fluid dynamics. Sci. Rep. 13, 7155.

Saraf, A.R., Yadav, S.P., 2018. 2 - fundamentals of bare-metal stents. In: Wall, J.G., Podbielska, H., Wawrzyńska, M. (Eds.), Functionalised Cardiovascular Stents. Woodhead Publishing, pp. 27–44.

Schmidt, W., Behrens, P., Schmitz, K.P., 2009. Biomechanical aspects of potential stent malapposition at coronary stent implantation. In: Dössel, O., Schlegel, W.C. (Eds.), World Congress on Medical Physics and Biomedical Engineering, September 7 - 12, 2009. Springer Berlin Heidelberg, Berlin, Heidelberg, Munich, Germany, pp. 136–139.

Schwartz, R.S., Topol, E.J., Serruys, P.W., Sangiorgi, G., Holmes Jr., D.R., 1998. Artery size, neointima, and remodeling: time for some standards. J. Am. Coll. Cardiol. 32, 2087–2094.

Serruys, P.W., de Jaegere, P., Kiemeneij, F., Macaya, C., Rutsch, W., Heyndrickx, G., Emanuelsson, H., Marco, J., Legrand, V., Materne, P., et al., 1994. A comparison of balloon-expandable-stent implantation with balloon angioplasty in patients with coronary artery disease. Benestent Study Group. N. Engl. J. Med. 331, 489–495.

Shen, D., Qi, H., Lin, W., Zhang, W., Bian, D., Shi, X., Qin, L., Zhang, G., Fu, W., Dou, K., Xu, B., Yin, Z., Rao, J., Alwi, M., Wang, S., Zheng, Y., Zhang, D., Gao, R., 2021a. PDLLA-Zn-nitrided Fe bioresorbable scaffold with 53-μm-thick metallic struts and tunable multistage biodegradation function. Sci. Adv. 7.

Shen, X.-Y., Barzegar Gerdroodbary, M., Abazari, A.M., Moradi, R., 2021b. Computational study of blood flow characteristics on formation of the aneurysm in internal carotid artery. Eur. Phys. J. Plus 136, 541.

Shen, X.-Y., Gerdroodbary, M.B., Poozesh, A., Musa Abazari, A., Imani, S.M., 2021c. Effects of blood flow characteristics on rupture of cerebral aneurysm: computational study. Int. J. Mod. Phys. C 32, 2150143.

Shen, X.-Y., Xu, H.-Q., Gerdroodbary, M.B., Valiallah Mousavi, S., Musa Abazari, A., Imani, S.M., 2021d. Numerical simulation of blood flow effects on rupture of aneurysm in middle cerebral artery. Int. J. Mod. Phys. C 33, 2250030.

Shen, X., Deng, Y.Q., Ji, S., Zhu, H.F., Jiang, J.B., Gu, L.X., 2019. Bending analysis of stented coronary artery: the interaction between stent and vessel. J. Mech. 35, 455–463.

Tofail, S.A.M., Koumoulos, E.P., Bandyopadhyay, A., Bose, S., O'Donoghue, L., Charitidis, C., 2018. Additive manufacturing: scientific and technological challenges, market uptake and opportunities. Mater. Today 21, 22–37.

Wang, C., Zhang, L., Fang, Y., Sun, W., 2021. Design, characterization, and 3D printing of cardiovascular stents with zero Poisson's ratio in longitudinal deformation. Engineering 7, 979–990.

Wang, Q., Fang, G., Zhao, Y., Wang, G., Cai, T., 2017. Computational and experimental investigation into mechanical performances of Poly-L-Lactide Acid (PLLA) coronary stents. J. Mech. Behav. Biomed. Mater. 65, 415–427.

Wang, T., Butany, J., 2017. Pathogenesis of atherosclerosis. Diagn. Histopathol. 23, 473–478.

Wu, W., Yang, D.Z., Qi, M., Wang, W.Q., 2007. An FEA method to study flexibility of expanded coronary stents. J. Mater. Process. Technol. 184, 447–450.

Xu, X., Awwad, S., Diaz-Gomez, L., Alvarez-Lorenzo, C., Brocchini, S., Gaisford, S., Goyanes, A., Basit, A.W., 2021. 3D printed punctal plugs for controlled ocular drug delivery. Pharmaceutics 13.

Yang, C.-S., Wu, H.-C., Sun, J.-S., Hsiao, H.-M., Wang, T.-W., 2013. Thermo-Induced shape-memory PEG-PCL copolymer as a dual-drug-eluting biodegradable stent. ACS Appl. Mater. Interfaces 5, 10985–10994.